HiSST: 3rd International Conference on High-Speed Vehicle Science Technology
14 -19 April 2024, Busan, Korea

RAM-ACCELERATOR FOR FUTURE LOW-ORBITING OPERATION

Daniele Di Martino[1], Elisa Di Paola [2], Vincenzo Allegra[3], Emanuele Rua[4], Abdul R. [5], Phanindra Peri[6], Antonella Ingenito[7], Luana Georgiana Stoica[8], Alessandro Di Marco[9]

[1,2,8, 9] ROMA3, University of Rome, Italy
[3]Thales Alenia Space, Rome, Italy
[4]Power and Electronics Subsystem Engineer Rome, Vaud, Svizzera
[5,6,7] School of Aerospace Engineering University of Rome "La Sapienza", Italy

Corresponding author: Antonella Ingenito
Email address: antonella.ingenito@uniroma1.it
Tel: +39 3346068243

Abstract

The increasing demand for access to space, driven by both governmental and private entities, requires a fundamental shift towards more cost-effective and efficient means of launching payloads. Currently, the launch market is predominantly dominated by staged expendable launch vehicles, characterized by excessive costs per kilogram of payload. In this context, the Gun Launch to Orbit (GLTO) concept emerges as a promising alternative, offering simplicity, reusability, and the potential for significantly increased payload fractions. However, it also meets substantial challenges, including the need to withstand high g-loads and intense heating during hypersonic trans-atmospheric flight. This paper aims to explore the feasibility of utilizing the ram accelerator, particularly the thermally-choked ram accelerator (TCRA), to launch medium-small satellites. The investigation delves into the performance characteristics of TCRA, examining its response to variations in fuel composition, pressure, temperature, barrel length, and combustion heat release. Moreover, the paper extends its study to the optimization of dynamic intake geometries within hypersonic orbital launchers. This aspect of the research aims to enhance fuel combustion efficiency by ensuring that the selected fuel enters the combustion chamber with the requisite properties. By employing sophisticated modelling techniques and computational simulations, the study explores various intake geometries and their impact on fuel characteristics, thus paving the way for enhanced performance and reliability in micro-satellite launches. In conclusion, this extended abstract encapsulates a multifaceted exploration of GLTO technology and its potential applications in launching small satellites. By addressing critical challenges and proposing innovative solutions, this research contributes to the ongoing quest for cost-effective and sustainable access to space, fostering new opportunities for exploration, scientific discovery, and commercial ventures beyond Earth's atmosphere.

---

[7]School of Aerospace Engineering University of Rome "La Sapienza", Rome 00138, Italy. antonella.ingenito@uniroma1.it

Keywords: *Space launchers, Ram accelerator, guns, Combustion, micro-satellite*

Nomenclature

Roman Symbols
A: cross sectional area of the tube bore [m^2]
a=gun acceleration [m/s^2]
Cp: specific heat at constant pressure [J/kg/K]
F: thrust [N]
h the specific enthalpy
m: projectile mass [m]
M: Mach number [-]
p: initial pressure of the gas mixture [Pa]
q: heat release [cal]
Q: non-dimensional heat release parameter [-]
T_1: temperature of the undisturbed propellant [K]
V projectile speed [m/s]
u the mass-averaged particle velocity,

Greek Symbols
Δ: change
g heat capacity ratio [-]
τ : non-dimensional thrust [-]

Superscripts and subscripts
i: initial conditions
f: final conditions
1: conditions ahead the gun
2: conditions behind the gun

1. Introduction

The ram accelerator is a chemically driven ramjet-in-tube-device that consists of a tube filled with a pressurized gaseous fuel-oxidizer mixture in which a sub-caliber projectile is accelerated. The concept proposed for future space launches of acceleration-insensitive payloads aims to significantly reduce current launch costs. Although it may resemble a conventional long-barreled cannon, its principle of operation is markedly different, bearing closer resemblance to that of a supersonic air-breathing ramjet engine. This device consists of a stationary tube filled with a combustible gaseous mixture, typically methane, hydrogen, oxygen, and diluents like nitrogen, at pressures ranging from 5 to 200 atm (approximately 5 to 200 bar), with frangible diaphragms used to seal off each end of the tube, containing the propellant. The projectile, resembling the center body of a ramjet, has a diameter smaller than the launch tube bore and is often equipped with guide fins to ensure proper centering within the tube.

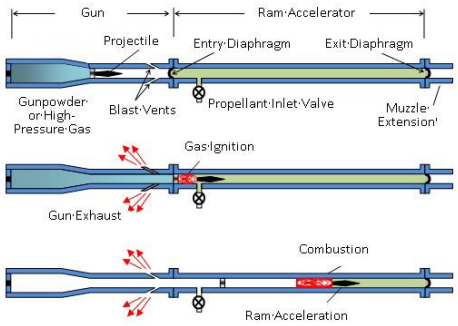

Fig 1. Operational sequence of ram accelerator [1]

To start a ramjet accelerator, an initial speed greater than 0.5 km/s must be imparted to the projectile. As the projectile moves forward, the premixed flow is compressed via reflected shock waves until pressure and temperature conditions are sufficient to allow flame anchoring. The projectile increases its speed until it reaches a maximum velocity, which is the Chapman-Jouguet (CJ) velocity. Under these conditions, the thrust is negligible, and therefore the velocity remains constant, and the ramjet cannot be further accelerated. The main difference between a ramjet accelerator and gun-like devices is that its source of energy is uniformly distributed along the entire length of the tube, whereas in a conventional gun, it is concentrated at the breech in the form of a charge of gunpowder or high-pressure gas. Since the launch parameters are independent of the initial conditions within the breech

of a gun, the projectile's acceleration and muzzle velocity can be quickly adjusted to specific needs by altering the propellant composition and the fill pressure in the launch tube.

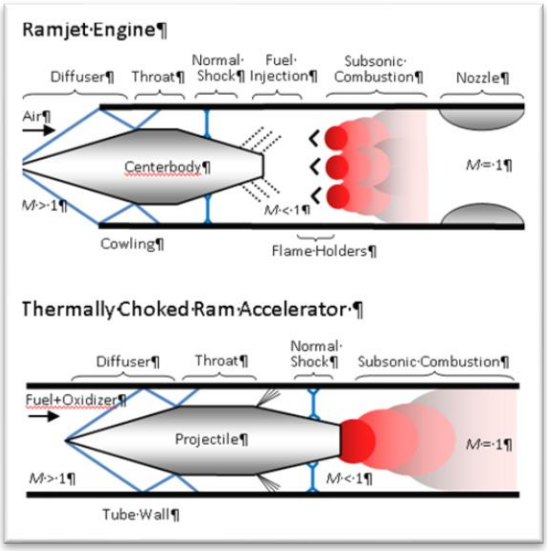

Fig 2. Ramjet Engine – Thermally Chocked Ram Accelerator [1]

This process generates thrust, increasing the base pressure on the projectile. In a conventional gun, the highest pressure is at the breech and the lowest is always at the base of the projectile. Instead, in the ram accelerator system, the highest pressure is always right behind the projectile, which is then accelerated down the tube[2-7]. The ram accelerator system has the advantage that the launch mechanism remains on Earth and does not have to be transported into space, as with a rocket. If the launcher is long enough, the acceleration can be reduced to a level that is compatible with current component technology, although the acceleration forces may prevent fragile payloads from being launched with feasible launcher lengths. Guns may therefore be limited to launching robust packages such as food, water, fuel, and replaceable components, or robust micro-satellites. This could serve as an important support function for the International Space Station (ISS) or other missions involving the use of micro-satellites.

1.1. Ram accelerator Concept: Sub-detonative Regime

The propulsive cycles of ram accelerators are classified based on the operating velocity regime. In the sub-detonative velocity regime, which is below the Chapman-Jouguet (CJ) detonation speed of the propellant, the combustion process typically takes place in a zone of subsonic flow relative to the projectile. This occurs downstream of a normal shock system stabilized behind the blunt base of the projectile, which acts as a flame holder. The release of combustion heat thermally chokes the flow in the entire tube area behind the projectile, stabilizing the shock system on it and isolating the flow around it from the turbulent expansion that occurs behind [5]. As a result, the pressure distribution on the vehicle generates forward thrust. By applying the steady flow conservation equations to a control volume containing the projectile, and assuming ideal gas behavior, the analytical solution for the non-dimensional thrust of the projectile can be derived [1, 2].

$$\rho_1 u_1 = \rho_2 u_2 \tag{1}$$

$$\rho_1 u_1^2 + p_1 + \frac{F}{A} = \rho_2 u_2^2 + p_2 \tag{2}$$

$$h_1 + \frac{u_1^2}{2} = h_2 + \frac{u_2^2}{2} \tag{3}$$

$$\tau = \frac{F}{pA} = \frac{\gamma_1 M_1}{\gamma_2 M_2}\left(1+\gamma_2 {M_2}^2\right)\left[\left(\frac{\gamma_2-1}{\gamma_1-1}\right)\left(\frac{1+\frac{(\gamma_1-1)}{2}{M^2}_1+Q}{1+\frac{(\gamma_2-1)}{2}{M^2}_2}\right)\right]^{\frac{1}{2}} - \left(1+\gamma_1 {M_1}^2\right) \quad (4)$$

The subscript 1 indicates the characteristics of the flow entering the control volume, while the subscript 2 refers to the flow exiting the control volume. Thermal choking of the flow behind the projectile implies that M2 = 1. The non-dimensional heat release parameter Q is given by [3]:

$$Q = \frac{\Delta q}{Cp_1 T_1} \quad (4)$$

This equation shows that the non-dimensional thrust τ is function of the heat non dimensional parameter Q, and consequently by the heat released by combustion, the initial temperature of the gas within the tube, and the TCRA length. The CJ velocity is strictly correlated to the initial pressure and temperature conditions.

2. TCRA analysis

The goal of this section is to analyze the non-dimensional thrust (τ) for different Q, p, T_1 and its sound speed a.

Most of the actual experimental ram accelerators are filled with mixtures based on methane (CH_4) and oxygen (O_2) as fuel with nitrogen (N_2) for dilution, with a large range of equivalence ratios [3] [4]. Figure 2 shows τ as function of the Mach number and the heat release parameter, assuming $\gamma_1 = \gamma_2 = 1.3$

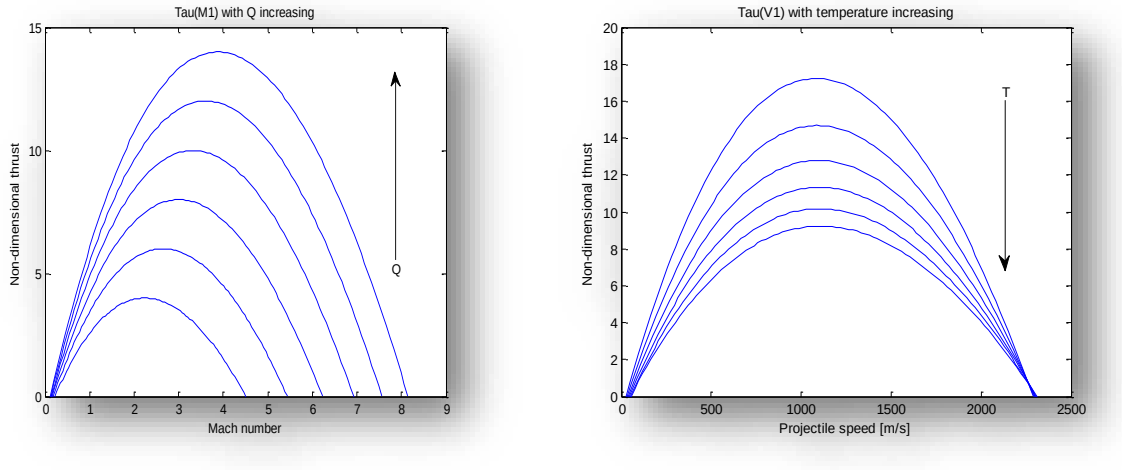

Fig 3. Non-dimensional thrust function of Mach number with heat release parameter ranging from 4 to 14; Non-dimensional thrust function of projectile speed with temperature ranging from 173 K to 323 K

The non-dimensional thrust increases with the Mach number till a maximum value, thence forward it starts decreasing, this is due to the increase of flow temperature for high Mach numbers. The thrust becomes void at the maximum detonation velocity of the propellant, called Chapman-Jouguet velocity. As Q increases, the non-dimensional thrust maximum increases as well and shifts towards higher Mach number, in fact the value of τ maximum for Q=4, is around M=2 meanwhile for Q=12 it is around M=4.

Combining eq. (1) with the following equations:

$$a = \sqrt{\gamma R T_1} \quad (10)$$

$$p = \rho R T_1 \quad (11)$$

The dependence of τ on temperature can be found.

Figure 3 shows that for lower temperature the peak of the non-dimensional thrust increases (as Q increases from eq. (4)). In particular temperature and maximum thrust are inversely proportional. Assuming a constant heat release parameter the increase of gas mixture pressure allows an increase of the projectile velocity peak and range, as shown in Fig. 4:

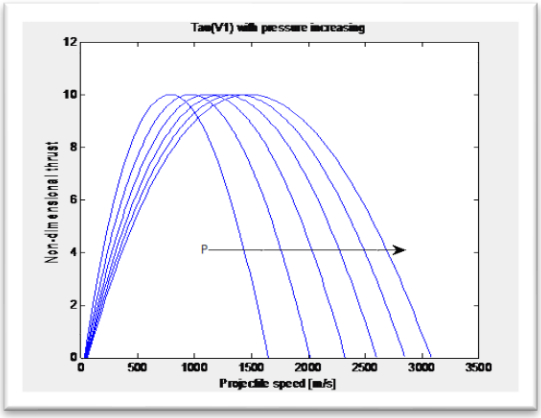

Fig 4. Non-dimensional thrust function of projectile speed with pressure ranging from 10 to 35 Mpa

In Fig. 3 and Fig. 4, $\tau = 0$ is in correspondence of to the higher possible speed, i.e., the CJ velocity and to the theoretical initial velocity. Actually, tests revealed that is necessary a speed quite higher than the theoretical initial velocity to start combustion and initiate the thermally choked propulsive mode. [5]
CJ and initial velocity values have been calculated finding the zero-points of the $\tau(V)$ function for different gas mixtures sound speeds (Table 1).
Table [1] shows the CJ velocity as function of the initial sound speed, pressure and velocities assuming a constant density of 60 kg/m^3 and non-dimensional heat release parameter of 10:

Table 1. Pressure, Initial velocity, and CJ velocity for certain values of gas mixture - sound speed (with Q=10 and density ρ=60 kg/m^3)

Sound speed [m/s]	**Pressure [MPa]**	**Initial velocity [m/s]**	**CJ velocity [m/s]**
300	4.15	43.31	2078.0
360	5.98	51.97	2493.6
420	8.14	60.63	2909.2
480	10.63	69.30	3324.8
540	13.46	77.96	3740.4
600	16.62	86.62	4156.0

Table [1] shows that increasing the sound speed, the CJ velocity increases as well, therefore it could be possible in principle consider a staged combustion, i.e., to use different propellant mixtures, with different molecular weights and therefore sound speeds. Assuming a sound speed of 500 m/s, initial and CJ velocities for different non-dimensional heat release parameters are shown in Table 2.

Table 2. Initial and CJ velocities for different values of the non-dimensional heat release parameter Q, a=500 m/s

Q	Vi [m/s]	Vcj [m/s]
6	91.95	2718.7
8	80.30	3113.4
10	72.18	3463.3
12	66.12	3781.0
14	61.37	4073.8
16	57.51	4347.0

In Table 2 are shown initial and CJ velocities for different non-dimensional heat release parameter values obtained with the same methodology, for constant sound speed.

2.1. TCRA length analysis

In this section, the total length of the barrel has been investigated for different gas mixture sound speeds and muzzle velocities. The possibility of minimize the length of a TCRA used for a certain range of velocity has been studied.
Given the variability of the acceleration, the length can be obtained from integral:

$$L = \frac{m}{pA}\int_{V_i}^{V_f}\frac{V_1}{\tau}dV_1 \tag{12}$$

m is the projectile mass, V_i and V_f the initial and the final values of V_1 - the projectile speed, and τ the non-dimensional thrust.

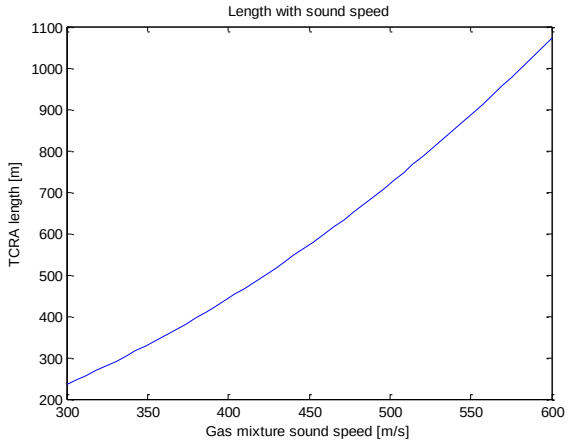

Fig 6. TCRA length function of gas mixture sound speed.

Assuming the projectile mass of 12000 kg, gas pressure of 10 MPa, barrel bore diameter of 1 m and non-dimensional heat release parameter of 10, the dependence of total length (that maximize the projectile velocity) on the mixture sound speed has been investigated (see Fig. 6). The TCRA length increases with the mixture sound speed. In fact, as the sound speed increases, the CJ velocity increases as well and consequently the maximum velocities accessible.
This explanation is also confirmed by Fig. 7. This figure shows that in order to have a muzzle velocity of 4000 m/s, a TCRA length of around 1 km is required and consequently a sound speed of 580 m/s.

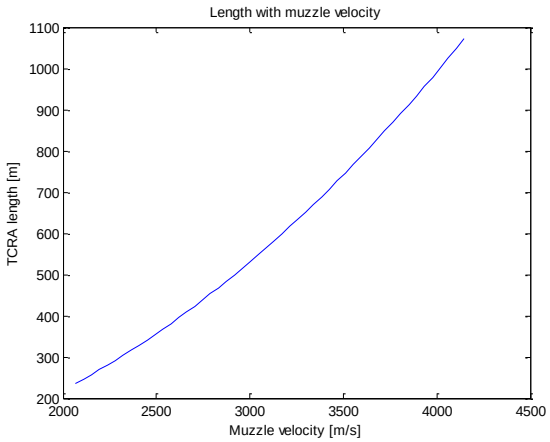

Fig 7. TCRA length function of muzzle velocity

The length barrel for the range of projectile, m=12000 kg, velocities between 1000 and 2500 m/s as function of gas mixture sound speed a has been investigated (Fig 8.), with pressure and heat release constraints (p=10 MPa and Q=10). There is an optimal sound speed for every range of speeds; in this case the optimal value can be detected in correspondence of the length minimum. TCRA total length can be decreased if the gas mixture sound speed varies during projectile acceleration, it can be obtained using different gas mixtures separated by diaphragms.

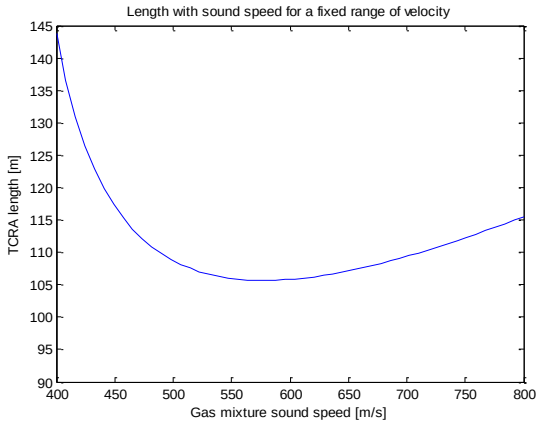

Fig 8. TCRA length with variation of sound speed for acceleration between 1000 and 2500 m/s.

3. Numerical Setup

The numerical setup was conducted through a two-dimensional Computational Fluid Dynamics (CFD) simulation, supplemented by a Matlab code describing the flow characteristics following variations due to shocks. Four geometries were selected, each of which was analyzed for four propellant mixtures. Operative conditions are as follows: M = 4, atmospheric temperature and pressure were set to T = 298K (25°C) and P = 101,325 kPa. The numerical model utilized is the SST k-omega model, and the simulation involves a mixture of CH4/air. The chemical model chosen for managing reactions is the Eddy-Dissipation model.

The geometries are described as follows:

• For the first geometry, the flow encounters an oblique shock at the leading edge of the intake, followed by an expansion wave at the point of inclination change, and an oblique shock upon exiting the intake at the truncation.

• For the second geometry, the flow encounters an oblique shock at the leading edge of the intake, an expansion wave at the beginning of the straight section, a reflection of the first oblique shock that falls into the straight section, another expansion wave at the point of inclination change at the end of the straight section, and an oblique shock upon exiting the intake at the truncation.

• For the third geometry, the flow encounters a first oblique shock at the leading edge of the intake, a second oblique shock at the beginning of the second ramp, an expansion wave at the point of inclination change, and an oblique shock upon exiting the intake at the truncation.

• For the fourth geometry, the flow encounters a first oblique shock at the leading edge of the intake, a second oblique shock at the beginning of the second ramp, an expansion wave at the beginning of the straight section, a reflection of the first oblique shock that falls into the straight section, another expansion wave at the point of inclination change at the end of the straight section, and an oblique shock upon exiting the intake at the truncation.

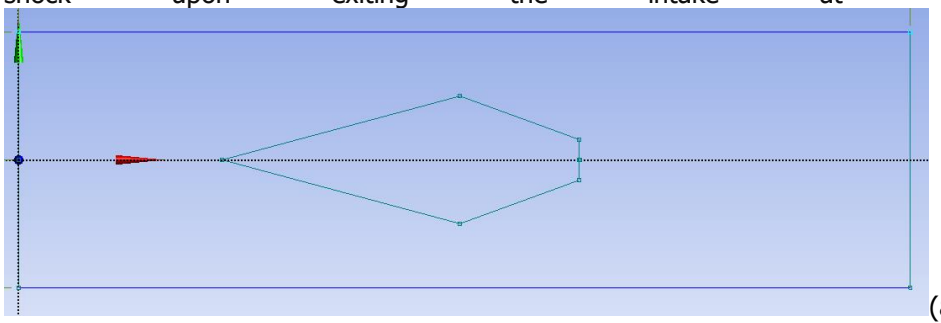
(a)

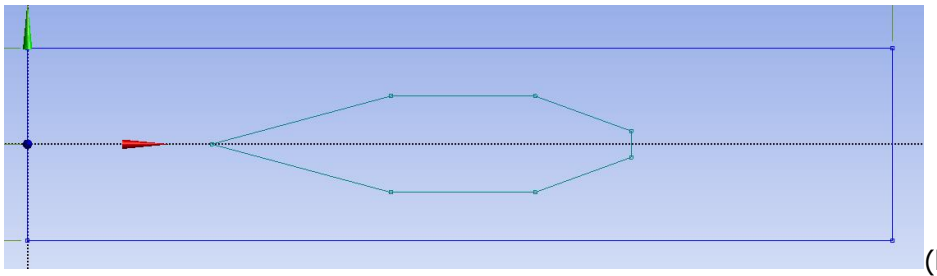
(b)

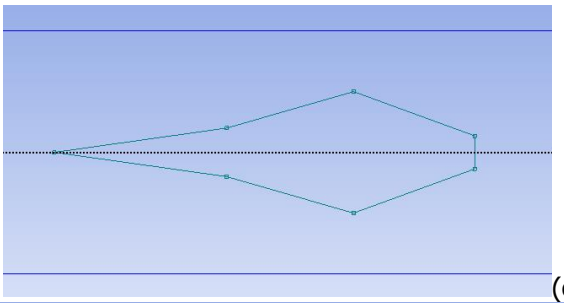
(c)

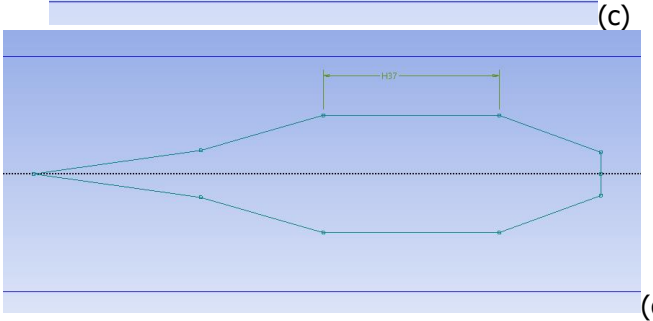
(d)

Fig 9. (a) first geometry, (b) second geometry, (c) third geometry, (d) fourth geometry

For each geometry analyzed, 4 propellants were studied (Table 3): $CH_4 + 2O_2$; $2.5CH_4 + 2O_2 + 4H_2$; $1.5CH_4 + 2O_2 + 7.5N_2$; $6H_4 + O_2$.

Table 3. Inlet characteristics of the mixtures.

	ρ [kg/m³]	γ	a[m/s]
$CH_4 + 2O_2$	1,091	1,362	355,6
$2.5CH_4 + 2O_2 + 4H_2$	0,5396	1,369	506,9
$1.5CH_4 + 2O_2 + 7.5N_2$	1,1085	1,384	355,6
$6H_4 + O_2$	0,1768	1,404	869,8

The conditions that the mixtures must meet to allow the starting of the combustion are as follows:

- The concentration of methane in the mixture must be between 5% and 15%.
- The concentration of hydrogen in the mixture must be between 4% and 75%.
- The minimum ignition temperature of CH4 + 2O2 must be 3053 K (2780°C).
- The minimum ignition temperature of 2.5CH4 + 2O2 + 4H2 must be 1536 K (1263°C).
- The minimum ignition temperature of 1.5CH4 + 2O2 + 7.5N2 must be 1904 K (1631°C).

3.1. Geometry results 1

The first geometry is depicted in Fig. 9(a). It has a total length of 2.8 m. The input half-angle is θ1 = 15º, while the output half-angle is θ2 = 2º. The central radius is 0.5 m, while at the truncation, it is 0.16 m. Here are the values of the output characteristics of the four mixtures for the first geometry:

Table 4. Characteristic results of the mixtures for the first geometry.

	Vspeed[m/s]	Pressure [Pa]	Temperature	Density [kg/m3]
CH_4+$2O_2$	771.81	1.55E+07	1710◦C	13,245
$2.5CH_4 + 2O_2 + 4H_2$	1098.7	2.33E+07	1749◦C	6,404
$1.5CH_4 + 2O_2 + 7.5N_2$	768.24	2.31E+07	1832◦C	12,543
$6H_4 + O_2$	1928,3	1.53E+07	1943◦C	1,881

Examining the results (Fig. 10 – Fig. 13), it becomes evident that all mixtures, except for the first one (refer to Table 4), meet the ignition conditions required for the combustion chamber, exhibiting acceptable pressure values. This indicates that the last three mixtures can be utilized with this geometry. The visual representations of the field characteristics obtained from the CFD simulation are arranged in adjacent positions.

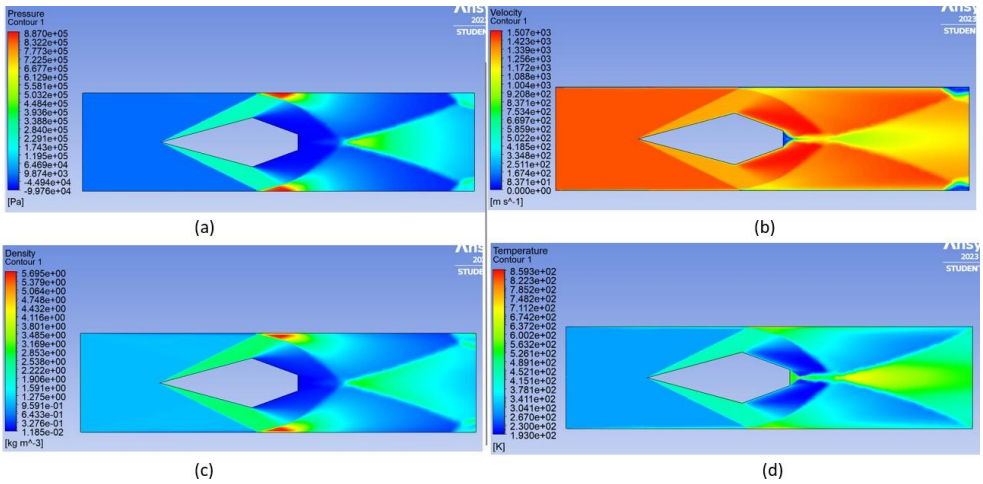

Fig 10. CFD representation of the feature field of the first geometry for CH_4 +$2O_2$: (a) Pressure; (b) Speed; (c) Density; (d) Temperature

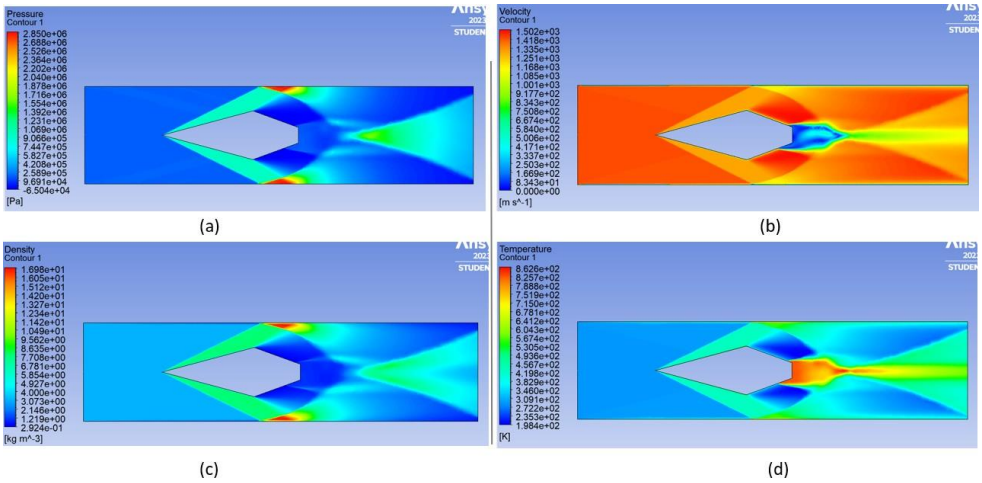

Fig 11. CFD representation of the feature field of the first geometry for $2.5CH_4+2O_2+4H_2$: (a) Pressure; (b) Speed; (c) Density; (d) Temperature

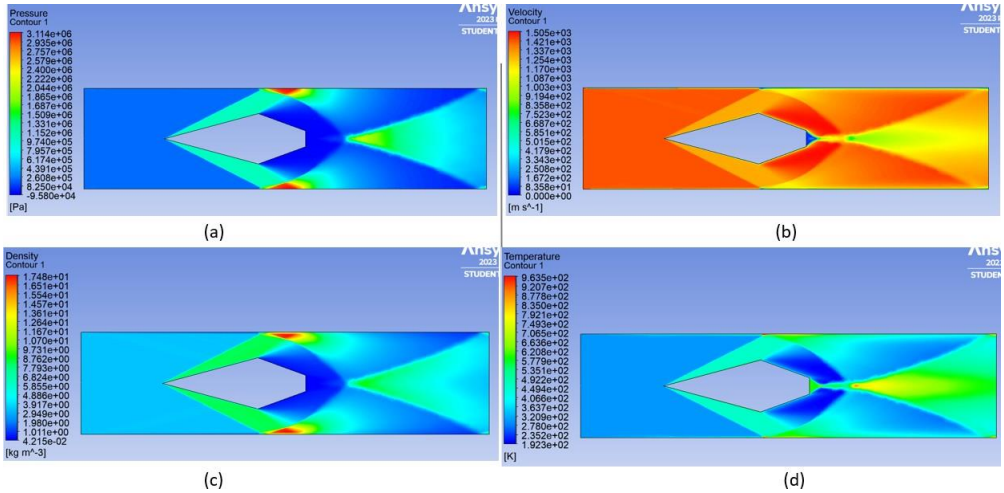

Fig 12. CFD representation of the feature field of the first geometry for $1.5CH_4+2O_2+7.5N_2$: (a) Pressure; (b) Speed; (c) Density; (d) Temperature

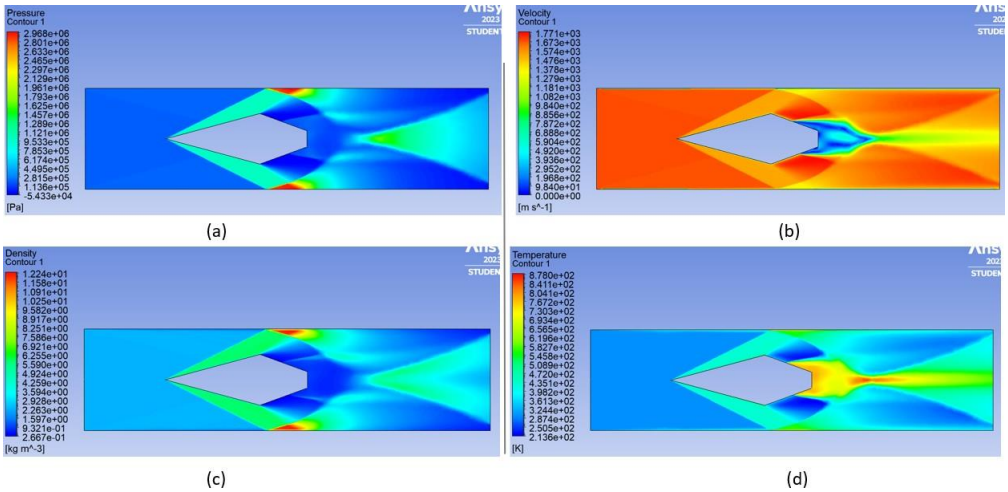

Fig 13. CFD representation of the feature field of the first geometry for $6H_4+O_2$: (a) Pressure; (b) Speed; (c) Density; (d) Temperature

3.2. Geometry results 2

The second geometry, depicted in (Fig. 14 – Fig. 17), features a total length of 4.4m. It has an input half-angle θ1 of 15 degrees, while the output half-angle θ2 is 20 degrees. The central radius is 0.5m, whereas at the truncation, it is 0.14m, with a straight treatment section of 1.5m. Utilizing the values from (Table 5), the subsequent results are derived.

Table 5. Characteristic results of the mixtures for the second geometry.

	Vspeed[m/s]	Pressure[Pa]	Temperature	Density[kg/m3]
CH_4+2O_2	745.88	6.92E+07	3207◦C	35,012
$2.5CH_4 + 2O_2 + 4H_2$	1061.3	1.03E+08	3290◦C	16,745
$1.5CH_4 + 2O_2 + 7.5N_2$	741.43	1.01E+08	3469◦C	32,056
$6H_4 + O_2$	1858.7	6.56E+07	3706◦C	4,666

All mixtures respect the ignition conditions in the combustion chamber. The second and third fuels have higher pressures. Since the barrel material may not withstand these pressures, structural damage may occur. The images of the feature fields obtained from the CFD simulation are placed side by side.

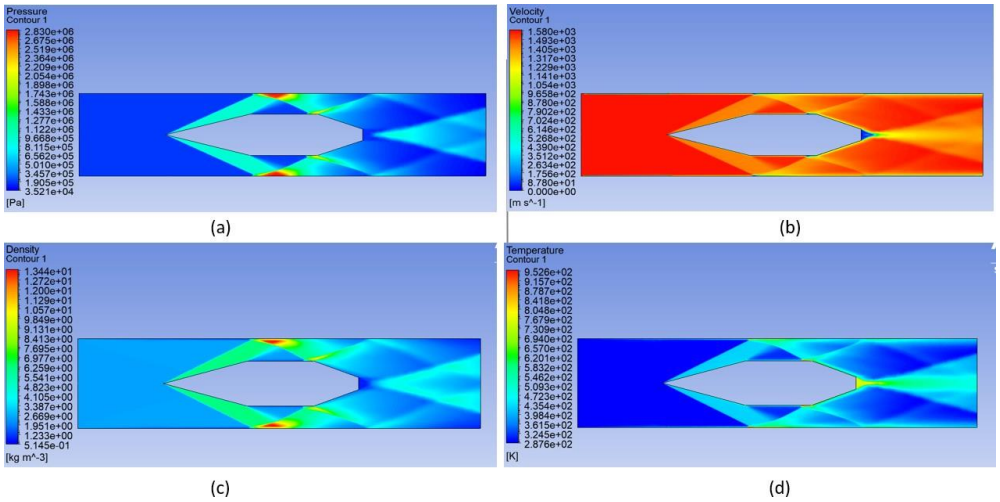

Fig 14. CFD representation of the feature field of the second geometry for CH_4+O_2: (a) Pressure; (b) Speed; (c) Density; (d) Temperature

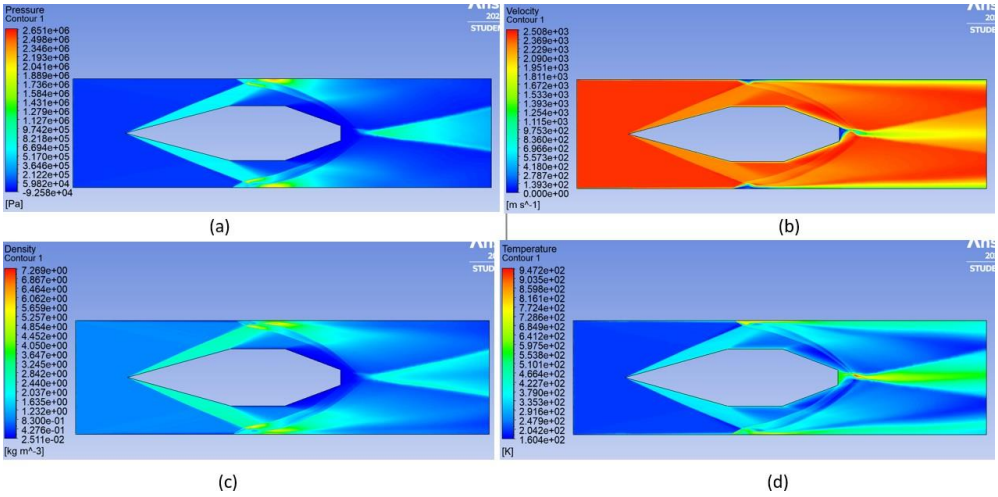

Fig 15. CFD representation of the feature field of the second geometry for $2.5CH_4+2O_2+4H_2$: (a) Pressure; (b) Speed; (c) Density; (d) Temperature

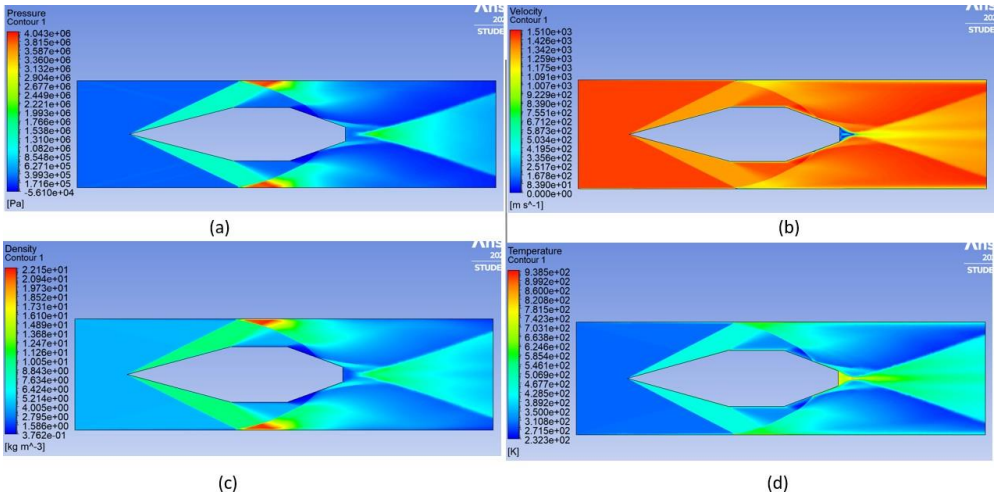

Fig 16. CFD representation of the feature field of the second geometry for $1.5CH_4+2O_2+7.5N_2$: (a) Pressure; (b) Speed; (c) Density; (d) Temperature

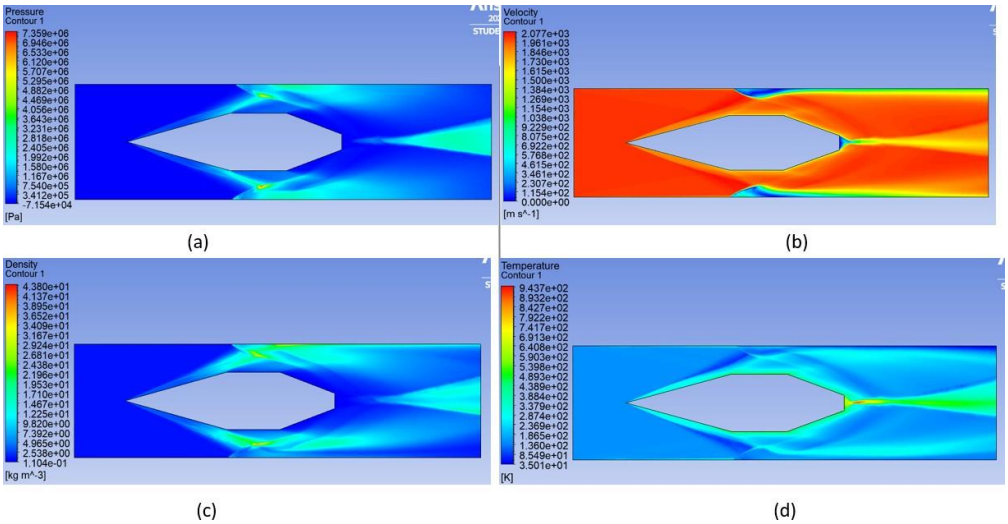

Fig 17. CFD representation of the feature field of the second geometry for $6H_4+O_2$: (a) Pressure; (b) Speed; (c) Density; (d) Temperature

3.3. Geometry results 3

The third geometry, shown in (Fig. 18 – Fig. 21), has a total length of 3.46m. The semi-angle of the first ramp is θ1 = 8◦, with a radius of 0.2m; that of the second ramp is θ2 = 16º, with a radius of 0.5m; while the output one θ3 = 20º, whose radius is 0.14m. Using the values from (Tab.6), the following results are obtained.

Table 6. Characteristic results of the mixtures for the third geometry

	Vspeed[m/s]	Pressure[Pa]	Temperature	Density[kg/m3]
CH_4+2O_2	671.31	1.95E+07	2487◦C	16,202
2.5CH_4 + 2O_2 + 4H_2	954.19	2.91E+07	2536◦C	7,783
1.5CH_4 + 2O_2 + 7.5N_2	655.17	2.86E+07	2641◦C	15,041
6H_4 + O_2	1662.9	1.87E+07	2776◦C	2,217

As for the first geometry, for this too it is possible to use all the mixtures studied except the first, which does not reach the ignition condition. The images of the feature fields obtained from the CFD simulation are placed side by side.

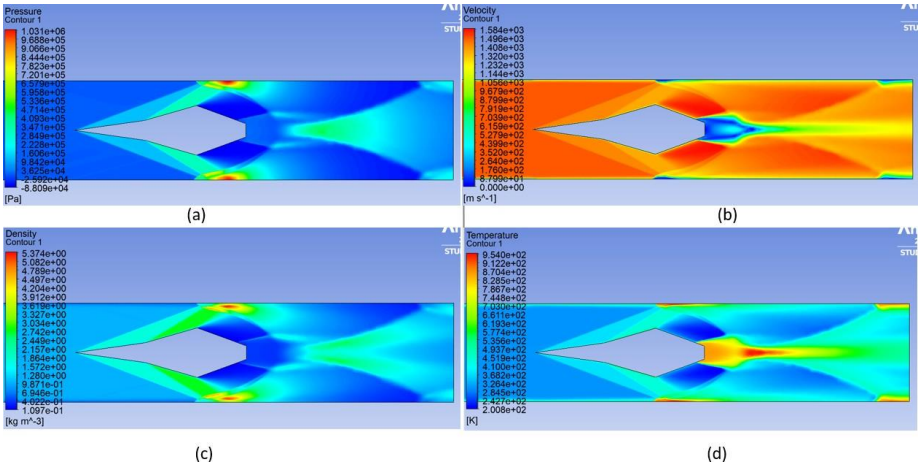

Fig 18. CFD representation of the feature field of the third geometry for CH_4+O_2: (a) Pressure; (b) Speed; (c) Density; (d) Temperature

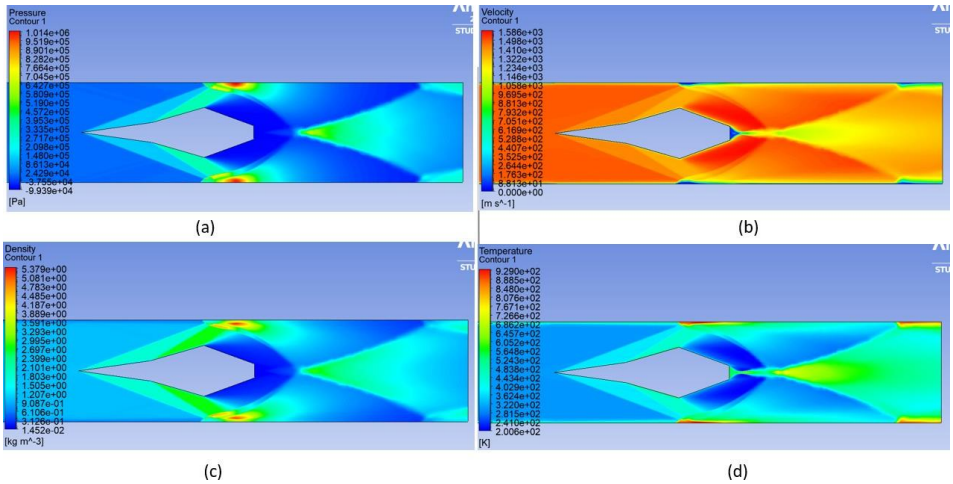

Fig 19. CFD representation of the feature field of the third geometry for 2.5CH_4+2O_2+4H_2: (a) Pressure; (b) Speed; (c) Density; (d) Temperature

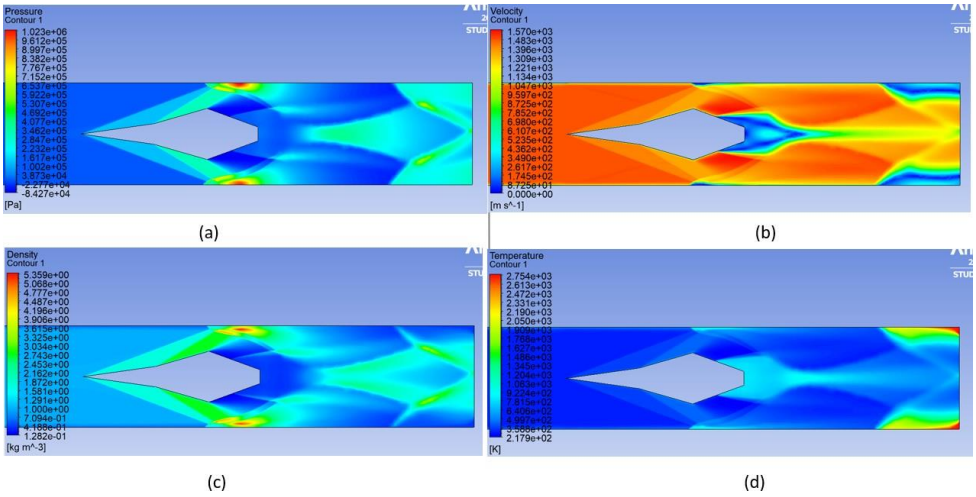

Fig 20. CFD representation of the feature field of the third geometry for $1.5CH_4+2O_2+7.5N_2$: (a) Pressure; (b) Speed; (c) Density; (d) Temperature

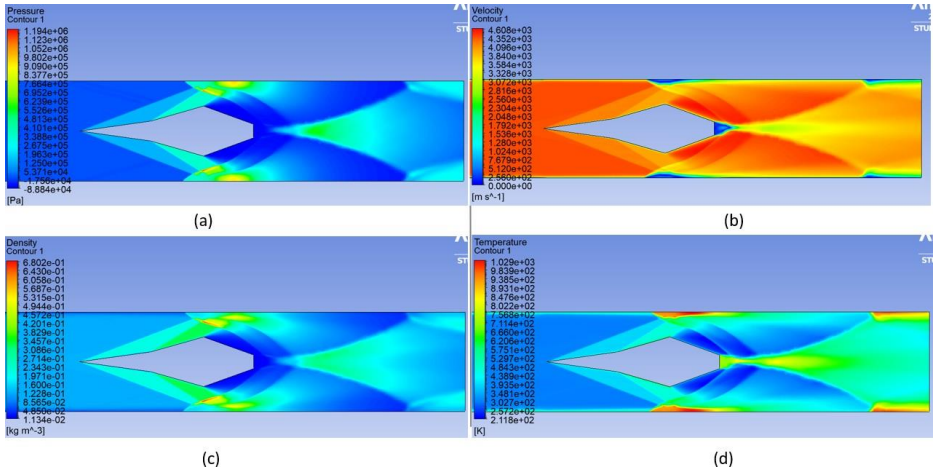

Fig 21. CFD representation of the feature field of the third geometry for $6H_4+O_2$: (a) Pressure; (b) Speed; (c) Density; (d) Temperature

3.4. Geometry results 4

The fourth geometry, shown in (Fig. 22 – Fig. 25), has a total length of 3.46m. The semi-angle from the Before ramp and θ_1 =8º, with a radius of 0.2m; that of the second ramp is θ2 = 16º, with a radius of 0.5m; while the output one θ3 = 20º, whose radius is 0.14m. The straight section is 1.5m long. Using the values from (Tab.7), the following results are obtained:

Table 7. Characteristic results of the mixtures for the fourth geometry

	Vspeed [m/s]	**Pressure [Pa]**	**Temperature**	**Density [kg/m3]**
***CH*$_4$ +2O$_2$**	687.23	1.05E+07	2310◦C	12,417
2.5CH4 + 2O2 + 4H2	977.04	1.55E+07	2346◦C	5,925
1.5CH4 + 2O2 + 7.5N2	681.43	1.5E+07	2421◦C	11,288
6H4 + O2	1704.6	9.58E+06	2512◦C	1,633

The fourth geometry also allows you to work with all mixtures except the first, since it does not reach the ignition condition. Furthermore, the mixture 6H4+ O2 has a lower pressure, albeit slightly, than other. This makes it preferable for this geometry as it creates stress on the rod material. The images

of the feature fields obtained from the CFD simulation are placed side by side.

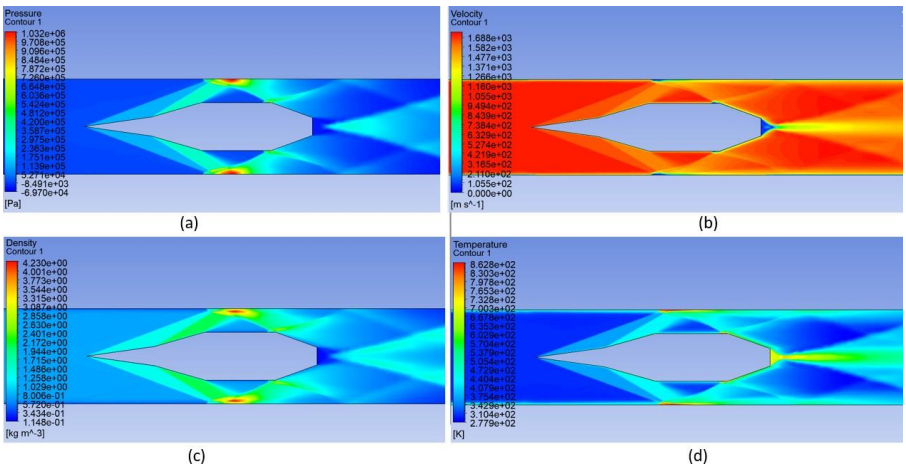

Fig 22. CFD representation of the feature field of the fourth geometry for CH_4+O_2: (a) Pressure; (b) Speed; (c) Density; (d) Temperature

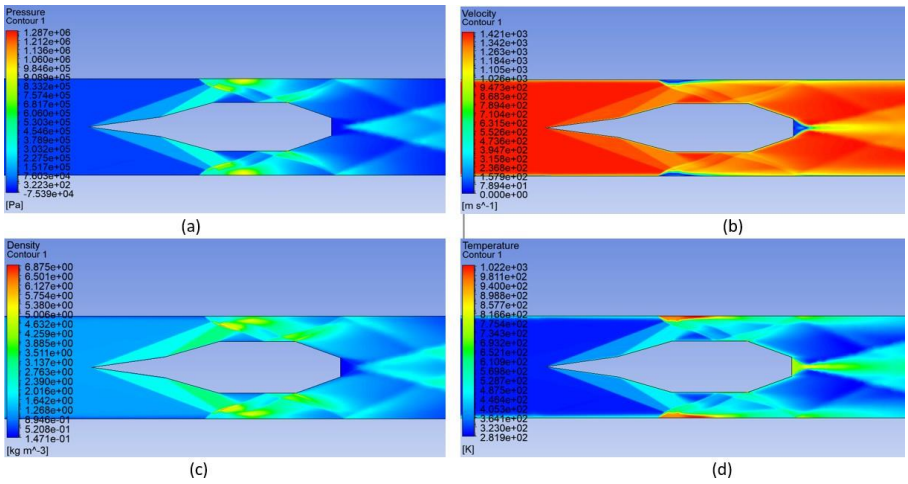

Fig 23. CFD representation of the feature field of the fourth geometry for $2.5CH_4+2O_2+4H_2$: (a) Pressure; (b) Speed; (c) Density; (d) Temperature

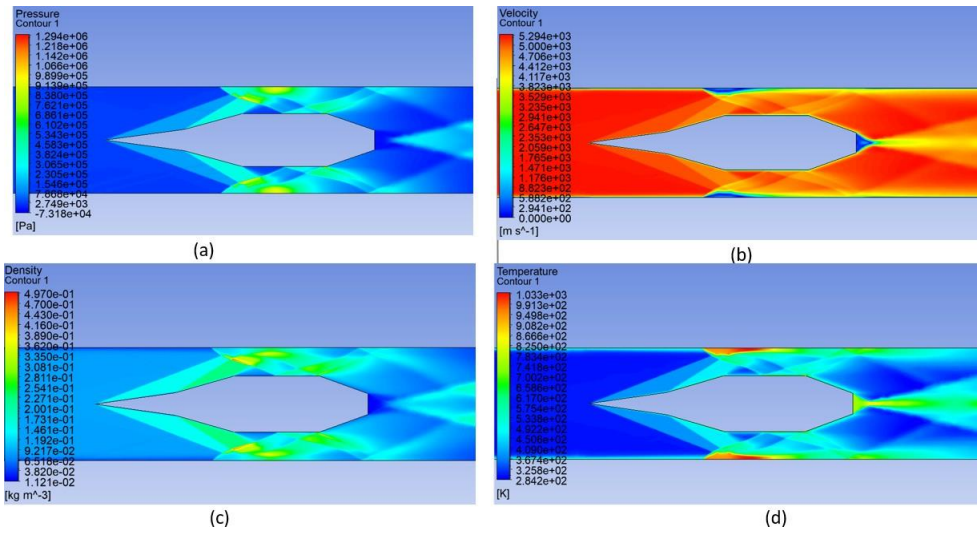

Fig 24. CFD representation of the feature field of the fourth geometry for

1.5CH_4+2O_2+7.5N_2: (a) Pressure; (b) Speed; (c) Density; (d) Temperature

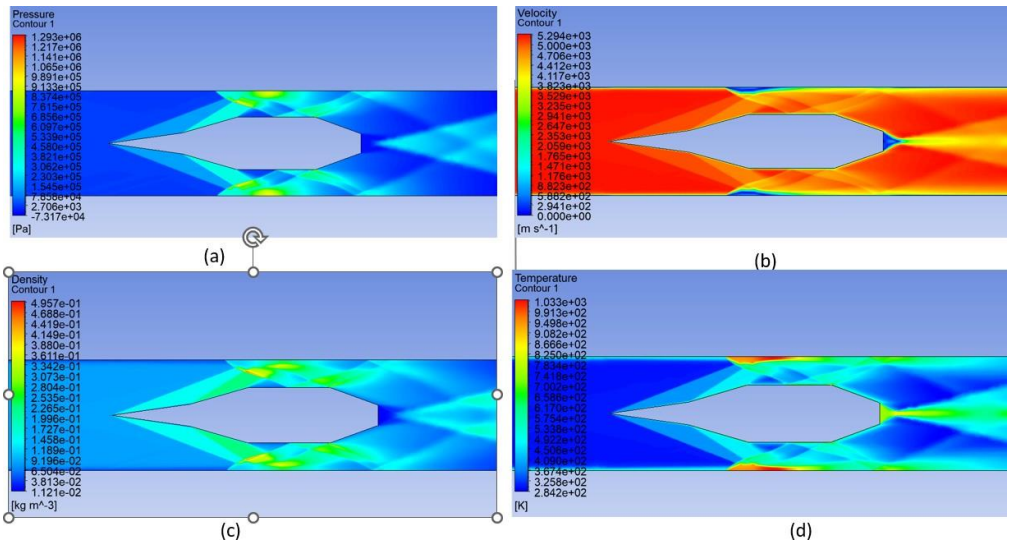

Fig 25. CFD representation of the feature field of the fourth geometry for 6H_4+O_2: (a) Pressure; (b) Speed; (c) Density; (d) Temperature

3.2. TCRA general design

In this section, requirements for launching a satellite with a TCRA and an additional rocket stage in Low Earth orbit are investigated.

2.3.1. LEO requirements

The necessary muzzle velocity to enter in a low earth orbit can be obtained from the energy conservation equation:

$$\frac{V^2}{2} - \frac{\mu}{r_e} = -\frac{\mu}{2r_e+h} \quad (13)$$

For a typical LEO at $h = 200\ km$ the launch speed is $V = 7.97\ km/s$ (through eq. (6). Launching eastbound the necessary variation of speed is $\Delta V = V - \bar{\omega}_e r_e = 7.5\ km/s$. Once reached the apogee of this elliptical orbit, the velocity will be $V_a = 7.72\ km/s$ (from eq. (6) and to obtain a circular orbit is a $V_c = 7.78$ km/s is required. The relative variation of speed ΔV implies a propellant mass that can be calculated with eq. (7):

$$m_p = m_s\left(e^{\frac{\Delta V}{g_0 Isp^{-1}}}\right) \quad (14)$$

g_0 is the gravity acceleration on earth surface, m_s the satellite dry mass, Isp the engine specific impulse.

2.3.2. TCRA and rocket stage

The practical limitations on TCRA muzzle velocities, due to the gas mixture CJ velocity, implies that the space launch with a ram accelerator is possible through a projectile provided with a rocket stage. Therefore is evaluated the possibility to launch the third and fourth stages of Vega – the light European launcher – replacing its first and second stages (P80 and Zefiro 23) with the ram acceleration.

Projectile characteristics are so assumed from Zefiro 9 and AVUM ones:

- Projectile mass: 13000 kg
- Projectile diameter: 2 m
- Vega 3rd stage ignition velocity: 3.8 km/s

- Vega 3rd stage ignition altitude: 135 km. [6] [7]

With a diameter ratio between projectile and bore of 0.77 the bore diameter must be about 2.6 m, resulting in a cross section A = 5.31 m^2.

The needed muzzle velocity can be obtained from eq. (6) applied between the real ignition point of Vega 2nd stage (Zefiro 9) and the hypothetical ignition point at the exit of the ram accelerator, on earth surface. It results to be of almost 4.2 km/s.

A muzzle velocity of almost 4.2 km/s can be reached with an ideal gas mixture with:

- Q = 12.
- Sound speed a = 551 m/s

In fact, with these values, the higher velocity of $\tau = 0$ is 4.25 km/s (as can be obtained from analysis of eq. (1)). The theoretical initial velocity is in correspondence of the other point of $\tau = 0$ and it is Vi = 71.4 m/s.

The other gas parameters are hypothesized (in respect of eq. (10)):

- R = 700 J/(kg*K)
- T = 310 K
- Heat ratio capacity $\gamma = 1.4$

Filling pressure influences length and density, for a pressure of 10 Mpa:

- TCRA length L = 438.1 m
- Gas mixture density $\rho = 46.08$ kg/m^3 (eq. (11)).

The maximum projectile acceleration is about 5000 g, it has been obtained from non-dimensional thrust peak with P, A and projectile mass.

The total gas mixture mass can be obtained from:

$$m_g = \rho A L \qquad (15)$$

To fill a similar TCRA are used around 107170 kg of gas mixture, comparable to P80 and Zefiro 23 propellant mass: 88365 kg + 23906 kg = 112271 kg with the difference that in TCRA case the propellant is basically gaseous hydrogen and oxygen meanwhile in Vega is solid [7]. The use of a TCRA with this configuration will be infrequent due to the large amount of propellant required; the concept for an optimal use of a TCRA is based on frequent launches, so on lower gas mixture total mass; to reach this goal a little projectile mass is required. Microsatellites are the ideal payload for a ram accelerator launching system, with small masses and low altitude orbits they allow a good launch frequency. With the goal of a 200 km high orbit and a payload of only 100 kg, the propellant mass required in the additional rocket stage and for the orbit circularization (for an engine of 1000 kg with a specific impulse of 400 s) is about 1625 kg. The total projectile mass will be around 2725 kg. With the same parameters of the previous case and for a muzzle velocity of 4000 m/s, the TCRA length will be of 98 m (with a bore diameter of 2 m) and the total gas mass of 14200 kg. In this case frequent shots are possible and a TCRA system will be justified from an economical point of view.

Since the increase of pressure linearly increases the mixture density and decreases the barrel length, the gas mixture mass is not affected by this parameter. Using a better gas mixture (increasing its sound speed or its heat release parameter) or reducing muzzle velocity allows a barrel length decrease.

A better TCRA optimization could be reached with the use of different gas mixtures during the projectile acceleration, with the purpose of keeping the non-dimensional thrust near its maximum. However, separation of the different gas mixtures and its effects on projectile acceleration when it transits

between gases separation surfaces will be critical issue to be explored [8].

Conclusion

This analysis has shown that the TCRA performance depends mainly on the Q and a gas mixture parameter, since these allow high muzzle velocities. A muzzle velocity of around 4000 m/s can be reached with the use of a hypothetical hydrogen-based mixture with R = 700 J/(kg*K) (i.e. $2H_2 + O_2$) and a non-dimensional heat release parameter Q = 12 (for H_2: R = 4124 J/(kg*K), $\gamma = 1.41$ [11]).

The propellant mass needed for ram acceleration can be compared with the propellant mass used by a modern launcher such as the Vega. The cost of a hydrogen-based mixture per kg and for its management will be high compared to actual costs for solid propellant, excluding the possibility of frequent launches.

Instead, the launch of microsatellites requires a ram accelerator length of less than 100 meters and less than 15 tons of propellant, therefore, in this way, launches can be frequent. Unlike actual space launchers, a TCRA will save costs for engines and disposable structures using the same barrel for different operations, actually the barrel is not subject to excessive wear due to the low velocities of the gas flow.

The best concept for future ram accelerated space launch remains the combined use of a TCRA and a SCRA which allows lower projectile masses, especially if improvements in the technical knowledge of the super-detonative propulsive mode will be achieved.

Ram acceleration is studied all over the world and continuous improvements are reached. Other technologies are not so much developed and do not seem to be next to a future implementation, also hypothesizing acceleration-insensitive payloads. Some of these devices have problems of relatively low efficiencies (like hypervelocity guns [12-14]), others have scaling problems.

References

[1] Douglas Witherspoon F., Kruczynski David L., Gun Launch to Space – A Discussion of Technology Options; UTRON Inc., Manassas, VA.

[2] Bruckner, A. P. and Hertzberg, A., "Ram Accelerator Direct Launch System for Space Cargo," 1987, 38th Congress of the International Astronautical Federation.

[3] Gilreath, H. E., Driesman, A. S., Kroshl, W. M., White, M. E., Cartland, H. E., , and Hunter, J. W., "Gun-Launched Satellites," JOHNS HOPKINS APL TECHNICAL DIGEST, Vol. 20, No. 3, 1999.

[4] Knowlen, Joseph, and Bruckner, "Ram Accelerator as an Impulsive Space Launcher: Assessment of Technical Risks," Tech. rep., 2007.

[5] Higgins, A. J., "Ram Accelerators: Outstanding Issues and New Directions," JOURNAL OF

[6] Shuxing Chen, Dening Li (2020), Conical shock waves in supersonic flow; Institute of mathematical research, Fudan University, China; Department of Mathematics, Wert Virginia University, USA.

[7] Dacheng Cui, Huicheng Yin (2008), Global supersonic conic shock wave for the steady supersonic flow past a cone: Polytropic gas; Department of Mathematics & IMS, Nanjing University, China.

[8] A. Hertzberg, A.P. Bruckner, C. Knowlen (1990), Experimental investigation of ram accelerator propulsion modes; Department of Aeronautics and Astronautics, University of Washington, USA;

[9] A.P. Bruckner, C. Knowlen, A.T. Mattick (1992), INVESTIGATION OF ADVANCED PROPULSION TECHNOLOGIES: THE RAM ACCELERATOR AND THE FLOWING GAS RADIATION HEATER, Aerospace and Energetics Research Program Department of Aeronautics and Astronautics, University of Washington, Seattle, WA.

[10] A.P. Bruckner (2002), The ram acelerator: a technology overview; Department of Aeronautics and Astronautics University of Washington, Seattle, WA.

[11] Carl Knowlen and Adam P. Bruckner, Direct Space Launch Using Ram Accelerator Technolog; Department of Aeronautics and Astronautics Aerospace and Energetics Research Program, University of Washington, Seattle, WA.

[12] Bogdanoff, D. W., "Ram Accelerator Direct Space Launch System: New Concepts," JOURNAL OF

PROPULSION AND POWER, Vol. 8, No. 2, 1992.

[13] Kruczynski, D., "High performance ram accelerator research," Tech. rep., 1997.

[14] Palmer, M. R., "Implications of a Gun Launch to Space for Nanosatellite Architectures," Tech. rep.